HHS Public Access

Author manuscript

Nat Neurosci. Author manuscript; available in PMC 2014 March 19.

Published in final edited form as:

Nat Neurosci. ; 15(7): 1047–1053. doi:10.1038/nn.3126.

pHTomato: A genetically-encoded indicator that enables multiplex interrogation of synaptic activity

Yulong Li[1] and **Richard W. Tsien**[1,2]

[1]Department of Molecular and Cellular Physiology, Stanford University School of Medicine, 279 Campus Dr., Stanford, CA 94305, USA

[2]NYU Neuroscience Institute and Department of Physiology and Neuroscience, New York University, New York, NY 10016, USA

Abstract

The usefulness of genetically-encoded probes for optical monitoring of neuronal activity and brain circuits would be greatly advanced by the generation of multiple indicators with non-overlapping color spectra. Most existing indicators are derived from or spectrally convergent on GFP. We generated a bright, red, pH-sensitive fluorescent protein, pHTomato, that can be used in parallel with green probes to monitor neuronal activity. SypHTomato, made by fusing pHTomato to the vesicular membrane protein synaptophysin, reports activity-dependent exocytosis as efficiently as green reporters. When coexpressed with the GFP-based indicator GCaMP3 in the same neuron, SypHTomato enabled concomitant imaging of transmitter release and presynaptic Ca^{2+} transients at single nerve terminals. Expressing SypHTomato and GCaMP3 in separate cells enabled the simultaneous determination of presynaptic vesicular turnover and postsynaptic sub- and supra-threshold responses from a connected pair of neurons. With these new tools, we observed a close size matching between pre- and postsynaptic compartments as well as interesting target-cell dependent regulation of presynaptic vesicle pools. Lastly, by coupling expression of pHTomato- and GFP-based probes with distinct variants of channelrhodopsin, we provided proof-of-principle for an all-optical approach to multiplex control and tracking of distinct circuit pathways.

Keywords

transmitter release; exocytosis; pHTomato; fluorescent protein; pH indicator; optogenetics; calcium; neuronal activity

Genetically encoded indicators have greatly advanced our ability to understand the complex physiology of neurons by allowing non-invasive monitoring of a variety of activity-regulated signals, including membrane potential [1, 2], Ca^{2+} [3,4, 5], Cl^{-} [6], and transmitter

Corresponding Authors: Dr. Yulong Li (yulong@gmail.com), Phone (650) 736-1610; Fax (650)-725-8021; Dr. Richard W. Tsien (richard.tsien@nyumc.org), Phone (646) 501-4520.

Accession Number: Sequences for pHTomato have been deposited in GENBANK with accession code JQ966306.

Author Contributions: Y. L. conceived and performed the experiments. R.W.T. supervised the project. Y.L. and R.W.T. analyzed the data and wrote the paper.

release [7, 8]. Regrettably, the majority of existing optical probes, which are based on GFP or on energy transfer between a pair of fluorescent proteins (FRET), have a large degree of spectral overlap that precludes them from being used in a multiplex fashion. The development of indicators that can be used in combination with GFP-based indicators would allow, for example, simultaneous imaging of multiple classes of neurons to understand information processing, or of pre- and postsynaptic activity to isolate the locus of different types of synaptic plasticity. In addition, recent breakthroughs with novel optogenetic agents such as channelrhodopsin-2 and halorhodopsin provide powerful ways to start or stop neuronal firing [9-11]. Combining these optical tools for controlling circuit function with novel optical indicators of activity would greatly enhance our ability to explore the natural behavior of neurons and synapses.

Pioneering work has harnessed a pH-sensitive variant of green fluorescent protein, pHluorin, fused to a vesicle protein, VAMP2, to probe the turnover of synaptic vesicles [7]. When a vesicle undergoes exocytosis, the pH of the vesicle lumen changes from 5.5 to 7.4, causing pHluorin-based probes exposed to the vesicle lumen to increase their fluorescence, thereby reporting presynaptic vesicle turnover. Color variants of pHluorin would complement the many GFP-based probes and allow dual channel acquisition of images. A prime candidate, the mOrange mutant M163K, has a suitable pK_a 7.5 [12], but displays undesirable photoswitching behavior [13] and correspondingly poor performance in imaging transmitter release. Other color variants of fluorescent proteins, including mKate, are spectrally distinct from GFP, but sometimes display photoswitching behavior [13], and display a pK_a of 6.0 [14], not optimal for detection of vesicle exocytosis[15].

Accordingly, we set out to develop a pH-sensitive indicator protein, spectrally distinct from GFP, with a pK_a specifically tuned to report vesicle exocytosis. Starting with the monomeric red fluorescent proteins mRFP/mStrawberry [16, 17], we performed DNA shuffling and semi-random mutagenesis (see methods). Through three rounds of evolution, we identified a bright pH-sensitive mutant (Fig. 1), termed pHTomato because its excitation (550 nm) and emission (580 nm) peaks are similar to Tomato variants from the mFruit series [17]. pHTomato contains six amino acid differences relative to mStrawberry (F41T, F83L, S182K, I194K, V195T and G196D). Notably, pHTomato contains a critical threonine at position 66, reminiscent of mRFP-Q66T [18].

Cuvette measurements of recombinant pHTomato (Fig. 1a) demonstrate that it is highly pH sensitive, with a pK_a close to 7.8 (Fig. 1b, c). Notably, while the emission intensity of pHTomato shows strong pH dependence, its excitation and emission waveforms are pH independent (Fig. 1b). Such spectral stability is critical for straightforward multiplexing of pHTomato with genetically encoded indicators of other colors.

We fused pHTomato to the lumenal domain of VAMP2 and characterized its properties in mammalian cells. When expressed in HEK cells, the VAMP2-pHTomato fusion showed a pH dependence that is identical to recombinant pHTomato alone (Fig. 1c), indicating fusion to VAMP2 did not perturb the pH sensitivity of pHTomato. In addition, when expressed in primary cultures of rat hippocampal neurons, VAMP2-pHTomato showed reversible

fluorescent increases in response to field stimulation (Fig. 1d), demonstrating the capability of VAMP2-pHTomato to report synaptic vesicle exo-and endocytosis.

Mindful that synaptophysin displays less background expression on the plasma membrane than VAMP2[19, 20], we used synaptophysin as the basis for an improved reporter of vesicular turnover, sypHTomato. We inserted the pHTomato sequence into the middle of the open reading frame, pointing the pHTomato moiety toward the vesicular lumen. To confirm that overexpression of sypHTomato does not alter vesicle turnover, we used activity-dependent FM dye uptake and destaining as an independent assay of endo- and exocytosis. Dye uptake in sypHTomato-positive nerve terminals and untransfected controls were statistically indistinguishable ($p>0.1$; Suppl. Fig. 2). Moreover, we observed a near-perfect overlap of the destaining trajectories for sypHTomato-transfected cells relative to control cells upon further stimulation to release the FM dye (Suppl. Fig. 2). Thus, sypHTomato overexpression does not produce deleterious effects on vesicular dynamics.

We subsequently co-expressed sypHTomato with synaptophysin-pHluorin (sypH) for a direct comparison of their performance in the same hippocampal neurons (Fig. 1e). Despite the slightly higher pK_a of pHTomato (7.8) relative to pHluorin (~7.3[7, 15]), sypHTomato and sypH practically performed equally well in reporting synaptic vesicle fusion, consistent with theoretical considerations[15]. The peak height of the fluorescence signal from sypHTomato correlated well with that of sypH over a wide range of activity (Fig. 1f). We performed NH_4Cl dequenching experiments[15] and estimated the surface fraction of sypHTomato at rest to be 8.1± 1.2% (n=207 synapses, 4 experiments), similar to that of sypH reported previously (7.5 ± 1.1 %[19], 9.1± 0.6 %[20]). Finally, the signal-to-noise ratio was similar for both probes, and each was able to detect exocytosis elicited by as few as 5 stimuli. Therefore, sypHTomato is a robust, genetically encoded indicator with capabilities matching those of existing probes.

The two color capability provides an immediate advantage in clarifying the intricate relationship between vesicle fusion and presynaptic calcium signaling. Both processes can be imaged concurrently in single nerve terminals by using sypHTomato along with green calcium indicators such as GCaMP3 [ref [21, 22]]. In cultured hippocampal neurons co-transfected with sypHTomato and GCaMP3, sypHTomato was found to be highly enriched in presynaptic boutons, while GCAMP3 was distributed more diffusely (Suppl. Fig. 1c). In response to depolarizing field stimulation (10 Hz, 10 s), transient increases were observed in both GCaMP3 and sypHTomato fluorescence (Fig. 2a). The responses from a single neuron (Fig. 2a) were quantified with respect to both time (Fig. 2b) and location (Suppl. Fig. 1d). Further analysis revealed that the sypHTomato and GCaMP3 responses showed distinct temporal patterns in various neuronal compartments: presynaptic puncta (Fig. 2a, yellow arrows), interbouton regions (white arrow heads) and somata (Suppl. 1d, open circles). Presynaptic boutons were defined by subsequent NH_4Cl challenges, which imposed an influx of NH_3 to neutralize intracellular compartments [23] (see Methods). Whereas GCaMP3 responses were observed in both presynaptic terminals and interbouton regions (Fig 2a), the sypHTomato response was confined to the presynaptic puncta (Fig. 2a). However, the GCaMP3 response at the time of stimulation is considerably enhanced in the vicinity of sypHTomato responses ($P<0.01$, bouton vs. interbouton, Fig. 2b), as also seen in plots of

fluorescent intensity along the length of an axon (Suppl. Fig. 1d). The close spatial overlap of the two signals is consistent with the well-documented enrichment of voltage-gated calcium channels (VGCCs) within synaptic boutons. Lateral spread of Ca^{2+} from the synaptic regions to the interbouton regions was presumably attenuated by sequestration and extrusion.

This dual-color optical imaging approach allows calcium levels and presynaptic release to be compared directly at the same synapses. We progressively varied the number of stimuli (5 to 60 stimuli, 20 Hz) and simultaneously monitored $GCaMP3_{pre}$ and sypHTomato signals (Fig. 2c). When these signals were scaled to allow comparison of their kinetics, the decaying phase of the sypHTomato signal significantly outlasted the transient $GCaMP3_{pre}$, declining ~10 times more slowly (Fig. 2d). The decay kinetics of sypHTomato signals arising from 5 stimuli were very similar to those arising from 40 (Suppl. Fig. 1e). Evidently, the ensemble rate of endocytosis was not significantly altered by moderate increases in neuronal activity under our conditions. To determine how the amount of exocytosis per action potential varied with activity, we plotted the peak amplitude of sypHTomato signal as a function of the number of stimuli (Fig. 2e). The amplitude increased linearly up to 40 stimuli (Fig. 2e, dashed line), corresponding to a nearly constant amount of vesicular turnover per action potential, 0.16±0.06 % per AP at 20 Hz. From the vantage point of neural signaling, this provides a compact description of how a number of action potentials can be encoded as the extent of exocytosis.

We went on to test whether larger synapses are particularly enriched in a specific channel type, using specific toxins to dissect the contributions of various voltage-gated Ca^{2+} channel types. The average contributions of the channels were remarkably consistent among synapses of different size within the same axonal tree studies (see Suppl Fig. 3, 4). We found no evidence for a bimodal distribution of channel types in which some synapses completely lacked P/Q- or N-type channels. It is conceivable that previous studies in similar hippocampal culture systems [24, 25] may have included contributions from inhibitory nerve terminals, now known to rely on either P/Q- or N-type channels to the exclusion of the other.

SypHTomato enabled us to visualize synaptic transmission from a presynaptic terminal onto a postsynaptic cell in a wholly optical system. Traditional approaches have often been limited to either pre- or postsynaptic optical measurements, or have used electrophysiology, which lacks some advantages of genetically encoded indicators. We expressed sypHTomato and GCaMP3 in separate hippocampal neurons (see Methods), and looked for synaptic contacts between sypHTomato-positive terminals (Fig. 3a, red) and GCaMP3-positive dendrites (Fig. 3a, green). Putative contact sites (Fig. 3b) displayed characteristic morphology, with prominent presynaptic varicosities (red) lying in spatially close proximity to GCaMP3-positive postsynaptic structures (green). In functional recordings that capitalized on the sensitivity of the optical probes, we found that most of the putative contacts were *bona-fide* active synapses (postsynaptic Ca^{2+} rises detected in 51 out of 63 synapses in 11 neurons). Closer examination of individual synapses revealed that most of the presynaptic boutons innervated spine-like postsynaptic structures (Fig. 3a, b). The

fraction of nerve terminals that targeted spines increased with synapse maturation (Suppl. Fig. 5c), as expected for hippocampal excitatory synapses.

We functionally characterized individual synaptic contacts with a combination of electrical stimulation and pharmacological intervention. Electrical stimulation of presynaptic somata, sufficient to drive the turnover of the readily releasable pool of vesicles (40 stimuli at 20 Hz, ref. [26]), was followed by a pulse of NH_4Cl, to transiently deacidify the entire synaptic vesicle compartment (Fig. 3c, top trace). The resulting sypHTomato fluorescent signal increase provided a rough indication of the total number of presynaptic vesicles. Similarly, we monitored the postsynaptic response to the same burst of exocytosis, and then the increase of GCaMP3 signal in the presence of ionomycin (Fig. 3c, bottom trace), a selective calcium ionophore that raises Ca^{2+} uniformly throughout the cell. The amplitude of the ionomycin response served as a proxy for postsynaptic spine volume.

We next sought to determine whether correlations exist between pre- and post-synaptic compartments. Plotting the presynaptic sypHTomato signal against the corresponding postsynaptic GCaMP3 signal at individual synapses revealed a high degree of "size-matching" [27, 28] between presynaptic compartment and postsynaptic target (Fig. 3d, R=0.8).

Do presynaptic neurons act in a cell-autonomous manner to distribute their synaptic vesicles between different target cells, or is this allocation also dependent on the target? Taking advantage of the dual-color photometry approach, we divided presynaptic terminals arising from a sypHTomato-labeled neuron into those targeting a particular postsynaptic neuron and those that did not. We quantified of the standard deviation (SD) of sizes of total vesicle pools (probed by NH_4Cl) and readily releasable pools (probed by 40 stimuli, 20 Hz). Presynaptic boutons sharing the same postsynaptic neuron were more consistent in SD than other presynaptic terminals from the same axon. Interestingly, we found that presynaptic boutons sharing the same postsynaptic target neuron have similar vesicular abundance (n =43 synapses, 7 neurons), with a relatively small scatter in their NH_4Cl-evoked vesicular signal (relative SD =0.4±0.1, $P<0.05$, t test), compared to nerve terminals targeting an assortment of postsynaptic neurons (n= 141 synapses). The vesicles in the readily releasable pool also showed a similar trend (relative SD=0.6±0.2, $P<0.05$). In comparison, the fraction of RRP per total vesicle pool (0.27 ±0.15 and 0.25 ±0.11), expressed as ratio of the peak response by 40 stimuli (20 Hz) to NH_4Cl did not differ according to their targets ($P>0.1$, t test). Because all the labeled nerve terminals arose from the same presynaptic neuron, the relative precise allocation of synaptic vesicles at synapses sharing the same target neuron implicates extrinsic signaling, possibly involving retrograde communication from the postsynaptic cell itself[29].

We next combined single cell electrical stimulation with dual-color imaging to interrogate synaptic transmission directly (Fig. 4a). Stimulation with 40 pulses at 20 Hz near the soma of the presynaptic neuron (Fig. 4a, red) resulted in a robust increase in fluorescence from sypHTomato terminals (Fig. 4b, control, presynaptic pseudocolor; 4c, red trace), consistent with the high reliability of action potential propagation. The postsynaptic glutamate receptors were in turn activated, leading to a nearly concurrent increase of the GCaMP3 signal in the postsynaptic dendrite immediately adjacent to the presynaptic terminals (Fig.

4b, 4c, control, postsynaptic ROI 1). The GCaMP3 signal was also observed throughout the dendrite (Fig. 4b, 4c, control, postsynaptic ROI 2). We interpreted this global dendritic calcium increase as an outcome of postsynaptic firing and opening of VGCCs throughout the neuron. To test this interpretation, we applied NBQX, a selective AMPA receptor antagonist, to reduce postsynaptic receptor activation and thus lower the drive for postsynaptic spikes. Indeed, NBQX confined the postsynaptic response, restricting it to the dendritic region just postsynaptic to the active terminal (ROI1, Fig. 4b, 4c), whereas no calcium signal was detected in a nearby postsynaptic region (ROI2, Fig. 4b, 4c, NBQX). We confirmed that this isolated calcium response was a result of NMDA receptor activation by verifying that APV, a selective NMDA receptor antagonist, completely abolished all postsynaptic responses (NBQX/APV, Fig. 4b, 4c). Thus, the all-optical approach was capable of achieving single-synapse resolution robustly, as confirmed in multiple pairs of excitatory neurons (Fig. 4d).

Finally, with multiple color variants of activity probes in hand, we explored the possibility of using a multiplex optical strategy for both direct control and readout of neuronal activity. Such a combination of optical approaches is unprecedented, but would be very powerful for non-invasive studies of synapse-specific regulation within neural circuits. This strategy is illustrated here by combining color variants of channelrhodopsin with probes of exocytosis with distinct spectral properties (Fig. 5a). Using a bicistronic T2A expression system[10] to drive co-expression of genetically encoded agents (Fig. 5a, right), we introduced ChR2 and vGluTpH, a pHluorin-tagged vesicular glutamate transporter that specifically labels glutamate-containing vesicles[30], into the same cultured hippocampal neurons. The ChR2 and vGluTpH were robustly co-expressed by the T2A linkage and correctly targeted to plasma membrane and synaptic vesicles respectively. For proof-of-principle, we employed a single beam of blue light (436-450 nm, blue bar in Fig. 5b) to activate ChR2 and to interrogate vGluTpH (Fig. 5b), noting that distinct wavelengths could be used for activation and interrogation under other circumstances (Suppl. Fig. 6b). The vGluTpH responded to exocytosis in excitatory neurons, elicited by electrical field stimulation (40 Hz, 2 s) (Fig. 5, left). In the same cells, raising the frequency of blue light illumination (increasing from 0.3 Hz to 5 Hz for 20 s) caused a marked increase in vGluTpH signal, indicating enhanced vesicle turnover (Fig. 5c, center). The light-driven response was blocked by bath application of TTX (Fig. 5c, right), demonstrating the requirement for action potentials (and subsequent opening of voltage-gated Ca^{2+} channels) to trigger vesicle fusion. In a similar experiment, the spectral alignment of VChR1 and pHTomato allowed us to use a beam of green light (546-566 nm, green bar in Fig. 5b) to co-activate VChR1 and sypHTomato (Fig. 5d). Once again, the synaptic monitor reported a light-driven, action potential-dependent increase in vesicular turnover. To assess the potential crosstalk between these two systems, we investigated the more difficult condition in which blue light might bleed through to activate VChR1, whose activation spectrum tails off incompletely in the blue (Fig. 5b). Delivering blue light to neurons transfected with VChR1-T2A-sypHTomato (Fig.5e) did not evoke a detectable response even at double the light intensity (Fig. 5e, center). As a positive control, the same cells responded robustly to elevating the frequency of green light pulses (Fig. 5e, right). These data established proof-of-principle for the application of T2A-linked expression of molecular tools for the control and readout of neural activity. The availability

of spectrally distinct variants for both stimulation and recording enables an all-optical strategy for parallel use in distinct neuronal populations.

Discussion

We have generated a bright, red, pH-sensitive, genetically-encoded probe termed pHTomato and constructed indicators based on this probe that enable imaging of neurotransmitter release. The new molecules were designed to overcome a number of technical obstacles that hamper the ability of existing techniques to elucidate the mechanisms of presynaptic regulation. For example, conventional postsynaptic electrical recordings, though sensitive, can be complicated by passive cable filtering, postsynaptic receptor trafficking, saturation or desensitization. FM dye imaging is capable of directly assaying presynaptic function, but dye uptake generally occurs at all functional synapses, hampering experiments that require cell-type specificity. SynaptopHluorin directly monitors presynaptic activity and, being genetically-encoded, provides neuronal specificity. However, it fluoresces in the green, and thus has spectral properties that overlap with those of many common probes. New indicators are clearly desirable to complement the strengths of existing probes for important signaling agents such as Ca^{2+}, cAMP, IP3, NO, and activated kinases and phosphatases.

Our design strategy was to screen new molecules based on bright and monomeric red fluorescent proteins that were already available. We generated a variant library by combining DNA shuffling of mStrawberry and mRFP with random error-prone PCR throughout the molecule and screened bright mutants for optimal pH sensitivity. The newly generated indicator, pHTomato is spectrally well-separated from GFP-based probes (excitation and emission peaks at 550 nm and 580 nm respectively), and is as bright as EGFP at neutral pH. Best of all, its excitation spectrum is highly pH-sensitive in the appropriate pH range (pK_a 7.8). Accordingly, pHTomato is extremely dim in quiescent vesicles (pH 5.5), but much brighter when the vesicle interior equilibrates with the extracellular medium (pH 7.4). mOrange2 recently has been applied to image vesicular turnover concurrently with calcium[21] or pHluorin probes[31], although its pKa (6.5) could be further optimized to improve signal-to-noise. Other pH-sensitive probes such as mNectarine[32] and pHRed[33] were recently identified, albeit without explicit motivation for tracking synaptic transmission. mNectarine is less bright than pHTomato and pHRed undergoes a pH-dependent change spectral shape that could be disadvantageous for concomitant use with other probes though useful for ratiometric imaging. In contrast, sypHTomato, derived from pHTomato, operates on the same principle as synaptopHluorin[7], and displays comparable performance in culture (Fig. 1). If anything, sypHTomato would be better-suited than green probes for imaging in brain tissue where light scattering falls off at longer wavelengths.

Having a red pH-sensitive probe enabled us to perform dual color imaging with another functional indicator to study neural communications in a multiplex fashion. We have demonstrated this potential usage in two ways. First, we were able to image sypHTomato together with GCaMP3 within the same cellular region. We were able to visualize activity-dependent calcium signals and the corresponding vesicular turnover with single synapse resolution. The critical spatial resolution allows us to study how different populations of

voltage-gated Ca^{2+} channels scaled according to the presynaptic size. We found that the deployment of P/Q- and N-type channels displayed remarkable consistency at glutamatergic synapses, despite large size variations between individual presynaptic terminals.

Second, we were able to mark the presynaptic neuron with sypHTomato and read out postsynaptic calcium response reported by GCaMP3. This configuration enabled the first genetically-encoded, all-optical visualization of pre-to-post chemical synaptic transmission at single synapses. We have observed a close size matching between pre-and postsynaptic boutons at the single synapse level, consistent with EM reconstruction studies from slice tissues[28]. Interestingly, we also uncovered results showing presynaptic terminals tend to have similar presynaptic mass (e.g. readily releasable pool or total vesicle pool) if they happen to share the same postsynaptic target. It has been suggested that extrinsic factors such as retrograde signals from postsynaptic neurons[34], local dendritic excitability[29], or signals from glial cells[35] might regulate the presynaptic release probability. Our results point to novel possibilities: presynaptic RRP or total vesicular pools might also be concurrently regulated. Finally, our ability to visualize pre- and postsynaptic responses under subthreshold or suprathreshold conditions opens doors to perform studies to decipher the locus of pre- or postsynaptic regulation of synaptic strength in slice or *in vivo*.

Perhaps the widest application of dual-color synaptic photometry will involve probing multiple pathways within neural circuits. Here, we take a critical first step: combining optogenetic photostimulation with optical monitoring. Our strategy satisfies two important requirements: (1) using a specific light stimulus to drive neuronal firing with channelrhodopsin and to query an optical reporter of neurotransmission and (2) using a second distinct optical stimulus to achieve firing and read out of a second pathway without crosstalk with the first. In practical terms, we achieved this by using blue light to trigger spiking with ChR2 and to monitor synaptic activity with GFP-based reporters, and green light to drive VChR1 and pHTomato based probes in parallel fashion. In principle, this approach can be extended to photo-excitation and monitoring of different classes of neurons *in situ*. Our sypHTomato-based multiplex system could readily be extended to two-photon imaging for in slice or *in vivo* studies[36]. Because two-photon excitation is generally ineffective in activating channelrhodopsins[37], photostimulation and optical readout could conceivably be controlled independently, for example, using ChR2 in conjunction with sypHTomato (Suppl. Fig. 6b). The availability of a red, pH sensitive synaptic probe provides a key component of more flexible and robust optical platforms for dissecting neural circuits *in situ*.

Methods

Molecular Biology and protein purification

mRFP/ mStrawberry and GCaMP3 constructs were kindly provided by R.Y. Tsien (HHMI & UCSD, CA) and L. Looger (Janelia Farms, Virginia), respectively. ChR2/vChR1, sypH and vGluTpH were kindly provided by K. Deisseroth (Stanford, CA), Y. Zhu (Chicago, IL) and R.H. Edwards (UCSF, CA), respectively. Evolution of pHTomato was by carried out by error prone PCR (epPCR) using GeneMorph II kit with equal amounts of mRFP and mStrawberry as templates. After DpnI treatment, the amplified fragment was cloned into

pBAD/His vector (Invitrogen, Carlsbad) and transformed into 10G supreme electrocompetent cells (Lucigen, WI). Two additional rounds of epPCR were performed using a pool template that came from a collection of previous transformed colonies (~300 colonies each time). Before final selection, single bacterial colonies were cultured overnight in 96 well plates induced with 0.2% arabinose (w/v, in LB). Screening for pH sensitivity was performed with a fluorescent plate reader (FLEXstation II, Molecular Devices, CA) with excitation and emission wavelengths set at 540 and 590 nm respectively. Emission ratios were calculated from data obtained from ~600 individual colonies in the presence of PBS (pH7.4) or PBS plus 60 mM Sodium Acetate (pH 5.0, pK_a=4.7). Plasmids from bacteria with higher ratios were extracted and sequenced.

VAMP2-pHTomato was created by PCR insertion of pHTomato into the C terminal of VAMP2 so that it would face the lumen of SVs. SypHTomato was created by insertion of pHTomato between positions 184 and 185 of rat synaptophysin sequence as previously described[20]. Mammalian expression vector of sypHTomato, vGluTpH, ChR2, VChR1 were first subcloned into pDONR221 or pDONR-P2R-P3 plasmids to generate entry vectors and later assembled with CMV promoter (in HEK cells/neurons) or aCaMKII promoter (in neurons) by the LR recombination reaction (Multisite Gateway, Invitrogen). T2A linkers were inserted into entry vectors of vGluTpH or sypHTomato by mutagenesis (Change-IT, USB).

Recombinant His-tagged pHTomato or EGFP were purified by Ni-NTA chromatography (Qiagen). Spectral measurements of pHTomato were performed with a FluoroMax3 spectrofluorometer (Horiba, NJ) with peak of excitation set at 550 nm and emission set at 580 nm. Titration of pH was performed with a series of pre-calibrated PBS or PBS+60 mM sodium acetate solutions. Quantum yield measurements were done in a Safire^2 system (Tecan) using Rhodamine 6G (QY=0.95 in ethanol) as a reference.

Cell Culture and Transfections

CA3-CA1 hippocampal neurons were cultured as previously described [38]. Both HEK cells and neurons were transfected with DNA by calcium phosphate methods. For cotransfections, same amount of sypH and sypHTomato driven by CMV promoter were used. For sequential transfections, individual plasmid were separated mixed with calcium chloride and phosphate buffer and applied to neuron sequentially with interval of 2 ~ 24 hrs. Neurons were typically transfected after 7-9 days in vitro (DIV) and experiments performed at 14-21 DIV. All animal protocols were in compliance with the Institutional Animal Care and Use Committee of Stanford University.

Imaging, electrical and optical stimulation

Neurons were perfused with Tyrode solution (containing 150 mM NaCl, 4 mM KCl, 2 mM $CaCl_2$, 2 mM $MgCl_2$, 10 mM glucose, 10 mM Hepes, 310–315 mOsm, with pH at 7.35). Switching of perfusion solution was carried out with a precision of <2 s. In some experiments, solutions contained 10 μM NBQX and 50 μM D-APV (Tocris Bioscience) to prevent possible recurrent activity and synaptic plasticity. HEK cells were perfused with Tyrodes with non-membrane permeable MES buffer (50 mM, pK_a =6.1) or PBS to gauge

the pH dependence of surface VAMP2-pHTomato intensity. Surface fraction of VAMP2-pHTomato is about 25% of the total protein measured by detergent permeabilization experiments (0.1% Triton X-100). For the pair imaging, control solution was similar to the Tyrode except with 0 mM $MgCl_2$ and 5 μM glycine to prevent the block of NMDA receptors. A sypHTomato-positive neuron was stimulated by a glass pipette or a concentric bipolar electrode (FHC) placed close to the soma of the neuron with a current strength of ~ 1 mA. For field stimulation, neurons were stimulated by 40 mA current passing through platinum electrodes. 1 ms pulse with different duration was applied. All experiments were performed at room temperature.

Image acquisition was conducted as previously described (Zhang et al., 2009). Briefly, neurons were imaged on a Nikon TE2000 microscope (40 ×, 1.3 NA objective) with an EMCCD camera (Cascade512B, Roper Scientific), controlled by METAMORPH 7.0 Software (Universal Imaging). Dual color imaging of sypHTomato and GCaMP3 was accomplished by using two excitation filters (475/22 for GCaMP3 and 556/20 for pHTomato). For light stimulation/imaging experiments, blue light excitation filter (FF438/24, Semrock) at intensity 0.7-3 $mWmm^{-2}$ (measured by a digital light meter, CETO) and orange light excitation filter at 1-4 $mW\ mm^{-2}$ (556/20, Chroma) were used to excite ChR2/vGluTpH and vChR1/sypHTomato respectively. A dual band dichroic mirror (FF493/574-Di01, Semrock), and a dual band emitter centered at 512 nm and 630 nm respectively (FF01-512/630-25, Semrock) were used to collect fluorescent light. The attenuation of excitation light intensity and/or switching between exciters was controlled by a DG4 (Sutter Instruments). The switching time between two channels was <2 ms. Exposure times were typically 40 ms - 250 ms, and images were collected at 1-10 Hz. Crosstalks between pHTomato and GCaMP3 channels were measured to be less than 6%. Photobleaching of pHluorin, GCaMP3 or pHTomato was corrected for by linear fitting of the baseline, as validated by experiments in the presence of 100 mM $CdCl_2$.

Imaging analysis

Images were analyzed by using ImageJ (NIH) and METAMORPH 7.0 Software (Universal Imaging). Regions of interests were identified by NH_4Cl application (50 mM, pH7.4), 600 stimuli at 10 Hz or ionomycin application. NH_4Cl is in equilibrium with H^+ and NH_3. Non-charged NH_3 rapidly diffuses through the plasma membrane and neutralizes the acidic pH in synaptic vesicles. The mask used is a circular selection of 9 pixels (~ 2 mm). ROIs with fluorescent increases >3 STD larger than neighboring background regions were selected and applied to all the rest of protocols. ROI data were extracted as ASCII files and further processed by Origin 7.0 (OriginLab, MA) or Matlab (MathWorks, MA). To effectively remove the background autofluorescence, in some experiments the images for sypHTomato and GCaMP3 channels were processed by calculating the intensity difference before and after NH_4Cl or ionomycin application respectively.

Calcium calibration

To calibrate the cytosolic calcium signal, F_{min} and F_{max} of GCaMP3 were obtained inside the same boutons at the end of the experiments using methods similar to those described before [39, 40]. F_{min} was obtained by treating the cells with 5 mM EGTA along with 10 mM

ionomycin, and F_{max} was obtained by treating the cells with the mixtures of 1 mM Ca and 10 mM ionomycin. The in situ F_{min} and F_{max} values were used to convert live cell data to the absolute calcium concentration using the formula

$$([Ca^{2+}]/K_d)^n=(f/F_{max}-1/R_f)/(1-f/F_{max}) \quad (1)$$

where $R_f= F_{max}/F_{min}$. K_d, R_f and n are inherent properties of the sensors. The K_d (133±30 nM), R_f (6.1±2.1) and n (3.9±0.6) were obtained by least-squares fitting of data from 11 cells to equation 1. The K_d and Hill coefficient were consistent with values previously reported for GCaMP2 and GCaMP3[22].

We performed *in situ* calibrations to test whether 40 stimuli at 20 Hz would saturate bulk calcium concentration reported by GCaMP3. Both stimulation for longer durations (60 stimuli at 20 Hz, Fig. 2c) or at higher frequency (40 stimuli at 50 Hz) elicited larger responses, indicating that GCaMP3 signal reflecting the volume average $[Ca^{2+}]$ had not reached a ceiling. In addition, retrospective calibration in ionomycin (1 mM free Ca^{2+}) yielded a larger fluorescence response, larger than that reflecting the peak $[Ca^{2+}]_{pre}$ (380 nM), again consistent with non-saturated $[Ca^{2+}]_{pre}$. Conservative calculation of the bulk Ca2+ level based on the calibration curve and the standard deviation of GCaMP3 signal [40] indicate the maximal underestimation of calcium level would be no larger than 30%.

Statistics

Coefficient of VARIATION = SD/mean

Shapiro-Wilk test was performed in Matlab (MathWorks, MA).

Supplementary Material

Refer to Web version on PubMed Central for supplementary material.

Acknowledgments

We thank Michael Lin for help with quantum yield measurements. This work was supported by grants from NINDS (NS074785), NIMH (MH064070), the Burnett Family Foundation, and Mathers Foundation. We thank John Emery for expert technical assistance and Li Li for help with transfections. We thank Liqun Luo and Tsien lab members especially Mike Tadross, Scott Owen, Hyokeun Park and Rachel Groth for helpful discussions throughout the execution of this project.

References

1. Siegel MS, Isacoff EY. A genetically encoded optical probe of membrane voltage. Neuron. 1997; 19:735–741. [PubMed: 9354320]
2. Mutoh H, Perron A, Akemann W, Iwamoto Y, Knopfel T. Optogenetic monitoring of membrane potentials. Exp Physiol. 2011; 96:13–18. [PubMed: 20851856]
3. Miyawaki A. Development of Probes for Cellular Functions Using Fluorescent Proteins and Fluorescence Resonance Energy Transfer. Annu Rev Biochem. 2010
4. Miyawaki A, et al. Fluorescent indicators for Ca2+ based on green fluorescent proteins and calmodulin. Nature. 1997; 388:882–887. [PubMed: 9278050]

5. Zhao Y, et al. An expanded palette of genetically encoded Ca(2) indicators. Science. 2011; 333:1888–1891. [PubMed: 21903779]
6. Kuner T, Augustine GJ. A genetically encoded ratiometric indicator for chloride: capturing chloride transients in cultured hippocampal neurons. Neuron. 2000; 27:447–459. [PubMed: 11055428]
7. Miesenbock G, De Angelis DA, Rothman JE. Visualizing secretion and synaptic transmission with pH-sensitive green fluorescent proteins. Nature. 1998; 394:192–195. [PubMed: 9671304]
8. Miesenbock G, Kevrekidis IG. Optical imaging and control of genetically designated neurons in functioning circuits. Annu Rev Neurosci. 2005; 28:533–563. [PubMed: 16022604]
9. Chow BY, et al. High-performance genetically targetable optical neural silencing by light-driven proton pumps. Nature. 2010; 463:98–102. [PubMed: 20054397]
10. Zhang F, et al. Red-shifted optogenetic excitation: a tool for fast neural control derived from Volvox carteri. Nat Neurosci. 2008; 11:631–633. [PubMed: 18432196]
11. Boyden ES, Zhang F, Bamberg E, Nagel G, Deisseroth K. Millisecond-timescale, genetically targeted optical control of neural activity. Nat Neurosci. 2005; 8:1263–1268. [PubMed: 16116447]
12. Shaner NC, et al. Improving the photostability of bright monomeric orange and red fluorescent proteins. Nat Methods. 2008; 5:545–551. [PubMed: 18454154]
13. Kremers GJ, Hazelwood KL, Murphy CS, Davidson MW, Piston DW. Photoconversion in orange and red fluorescent proteins. Nat Methods. 2009; 6:355–358. [PubMed: 19363494]
14. Shcherbo D, et al. Bright far-red fluorescent protein for whole-body imaging. Nat Methods. 2007; 4:741–746. [PubMed: 17721542]
15. Sankaranarayanan S, De Angelis D, Rothman JE, Ryan TA. The use of pHluorins for optical measurements of presynaptic activity. Biophys J. 2000; 79:2199–2208. [PubMed: 11023924]
16. Campbell RE, et al. A monomeric red fluorescent protein. Proc Natl Acad Sci U S A. 2002; 99:7877–7882. [PubMed: 12060735]
17. Shaner NC, et al. Improved monomeric red, orange and yellow fluorescent proteins derived from Discosoma sp. red fluorescent protein. Nat Biotechnol. 2004; 22:1567–1572. [PubMed: 15558047]
18. Jach G, Pesch M, Richter K, Frings S, Uhrig JF. An improved mRFP1 adds red to bimolecular fluorescence complementation. Nat Methods. 2006; 3:597–600. [PubMed: 16862132]
19. Granseth B, Odermatt B, Royle SJ, Lagnado L. Clathrin-mediated endocytosis is the dominant mechanism of vesicle retrieval at hippocampal synapses. Neuron. 2006; 51:773–786. [PubMed: 16982422]
20. Zhu Y, Xu J, Heinemann SF. Two pathways of synaptic vesicle retrieval revealed by single-vesicle imaging. Neuron. 2009; 61:397–411. [PubMed: 19217377]
21. Li H, et al. Concurrent imaging of synaptic vesicle recycling and calcium dynamics. Front Mol Neurosci. 2011; 4:34. [PubMed: 22065946]
22. Tian L, et al. Imaging neural activity in worms, flies and mice with improved GCaMP calcium indicators. Nat Methods. 2009; 6:875–881. [PubMed: 19898485]
23. Boron WF, De Weer P. Intracellular pH transients in squid giant axons caused by CO2, NH3, and metabolic inhibitors. J Gen Physiol. 1976; 67:91–112. [PubMed: 1460]
24. Reuter H. Measurements of exocytosis from single presynaptic nerve terminals reveal heterogeneous inhibition by Ca(2+)-channel blockers. Neuron. 1995; 14:773–779. [PubMed: 7718239]
25. Reid CA, Clements JD, Bekkers JM. Nonuniform distribution of Ca2+ channel subtypes on presynaptic terminals of excitatory synapses in hippocampal cultures. J Neurosci. 1997; 17:2738–2745. [PubMed: 9092595]
26. Murthy VN, Stevens CF. Reversal of synaptic vesicle docking at central synapses. Nat Neurosci. 1999; 2:503–507. [PubMed: 10448213]
27. Pierce JP, Lewin GR. An ultrastructural size principle. Neuroscience. 1994; 58:441–446. [PubMed: 8170532]
28. Harris KM, Stevens JK. Dendritic spines of CA 1 pyramidal cells in the rat hippocampus: serial electron microscopy with reference to their biophysical characteristics. J Neurosci. 1989; 9:2982–2997. [PubMed: 2769375]

29. Branco T, Staras K, Darcy KJ, Goda Y. Local dendritic activity sets release probability at hippocampal synapses. Neuron. 2008; 59:475–485. [PubMed: 18701072]
30. Voglmaier SM, et al. Distinct endocytic pathways control the rate and extent of synaptic vesicle protein recycling. Neuron. 2006; 51:71–84. [PubMed: 16815333]
31. Ramirez DM, Khvotchev M, Trauterman B, Kavalali ET. Vti1a Identifies a Vesicle Pool that Preferentially Recycles at Rest and Maintains Spontaneous Neurotransmission. Neuron. 2012; 73:121–134. [PubMed: 22243751]
32. Johnson DE, et al. Red fluorescent protein pH biosensor to detect concentrative nucleoside transport. J Biol Chem. 2009; 284:20499–20511. [PubMed: 19494110]
33. Tantama M, Hung YP, Yellen G. Imaging intracellular pH in live cells with a genetically encoded red fluorescent protein sensor. J Am Chem Soc. 2011; 133:10034–10037. [PubMed: 21631110]
34. Micheva KD, Buchanan J, Holz RW, Smith SJ. Retrograde regulation of synaptic vesicle endocytosis and recycling. Nat Neurosci. 2003; 6:925–932. [PubMed: 12910242]
35. Auld DS, Robitaille R. Glial cells and neurotransmission: an inclusive view of synaptic function. Neuron. 2003; 40:389–400. [PubMed: 14556716]
36. Helmchen F, Denk W. Deep tissue two-photon microscopy. Nat Methods. 2005; 2:932–940. [PubMed: 16299478]
37. Rickgauer JP, Tank DW. Two-photon excitation of channelrhodopsin-2 at saturation. Proc Natl Acad Sci U S A. 2009; 106:15025–15030. [PubMed: 19706471]
38. Zhang Q, Li Y, Tsien RW. The dynamic control of kiss-and-run and vesicular reuse probed with single nanoparticles. Science. 2009; 323:1448–1453. [PubMed: 19213879]
39. Kao JP, Harootunian AT, Tsien RY. Photochemically generated cytosolic calcium pulses and their detection by fluo-3. J Biol Chem. 1989; 264:8179–8184. [PubMed: 2498309]
40. Maravall M, Mainen ZF, Sabatini BL, Svoboda K. Estimating intracellular calcium concentrations and buffering without wavelength ratioing. Biophys J. 2000; 78:2655–2667. [PubMed: 10777761]

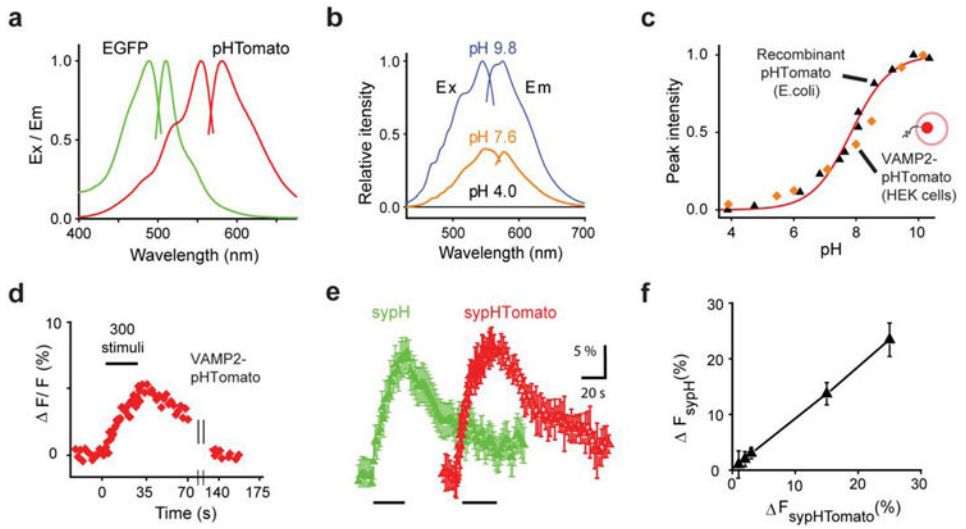

Figure 1. pHTomato spectra and properties

(a) Excitation and emission spectra for EGFP and pHTomato. Spectral peaks of pHTomato (excitation, 550 nm, emission 580 nm) are well separated from those of EGFP. (b) pH-dependence of pHTomato fluorescence; no change in wavelength of excitation and emission peaks. (c) Normalized fluorescence intensity of recombinant pHTomato and VAMP2-pHTomato were both highly pH-dependent, with identical values of pK_a (7.8±0.1). (d) VAMP2-pHTomato reported activity-dependent exo/endocytosis in cultured hippocampal neurons, reflected by stimulus-driven rise and fall in fluorescence signal. (e) Quantification of fluorescent signals from synaptophysin-pHluorin (sypH) and sypHTomato, expressed in the same neuron. Both probes performed equally well in reporting presynaptic activity as ΔF/F. Data obtained by averaging responses of 110 boutons (300 stimuli at 10 Hz). Traces displaced horizontally for clarity. (C) Comparison of sypH and sypHTomato signals under different stimulation conditions, ranging from 5 to 1200 stimuli, n=6 neurons, ~700 boutons) shows their proportional and nearly equal responses. All error bars are s.e.m.

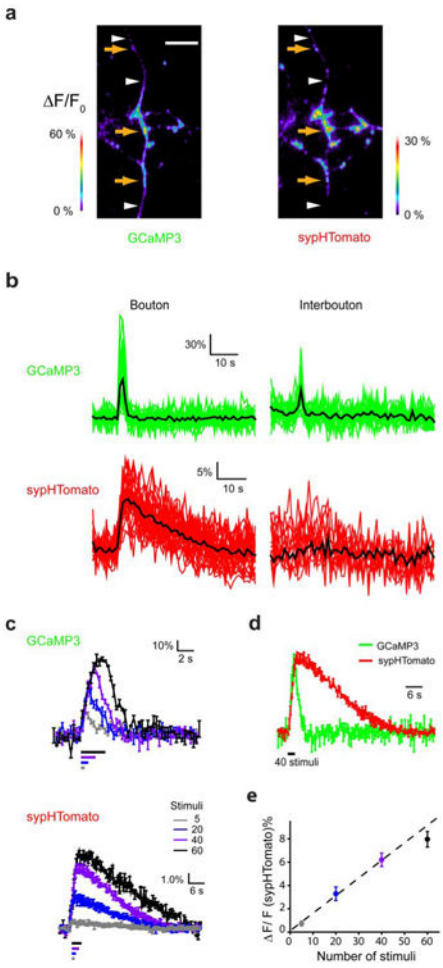

Figure 2. Dual color simultaneous imaging of vesicle fusion and cytosolic Ca^{2+}

(a) Pseudocolor snapshots of ΔF/F fluorescence signals evoked by 100 stimuli (10 Hz) for GCaMP3 and sypHTomato, respectively. Arrows indicate putative presynaptic boutons; arrowheads indicate inter-bouton regions. Scale bar, 10 μm. (b) Collection of GCaMP3 and sypHTomato responses over time from 20 putative presynaptic boutons (randomly selected out of 152 in total) and corresponding adjacent inter-bouton regions ~2-5 μm away. Averages of individual traces shown in black. Responses evoked with 40 stimuli at 20 Hz. The data are from the cell shown in (a). (c) Average GCaMP3 and sypHTomato signals from a set of synapses in response to trains of 5, 20, 40 and 60 stimuli (20 Hz). Each trace represents pooled data from ~600 boutons on five different coverslips. Error bars, S.E.M. (d) Comparison of kinetics of GCaMP3 and sypHTomato signals in response to 40 stimuli at 20 Hz. Note that the decay of averaged sypHTomato signal ($\tau_{sypHTomato}$ = 15.5 ± 0.5 s) significantly outlasted that of the presynaptic GCaMP3 response (τ_{GCaMP3} = 1.5 ± 0.14 s). (e) Quantification of peak amplitudes of sypHTomato responses. All data conform to regression line passing through the origin, showing linear increase with the number of stimuli, apart from fall-off at 60 stimuli. Thus, response amplitude per AP stays the same up to 40 stimuli (p>0.2). All error bars are s.e.m.

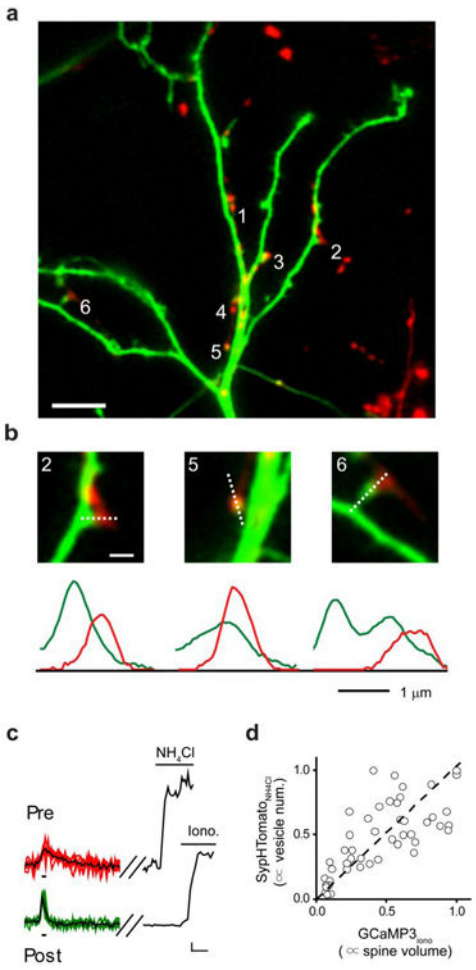

Figure 3. Dual color imaging of synaptic connection by sypHTomato and GCaMP3

(a) Image of a pair of connected neurons (DIV 20) where pre- and postsynaptic neuron expressed sypHTomato (red) and GCaMP3 (green). Regions 1∼ 6 highlight some putative synapses. Scale bar, 10 μm. (b) Enlarged views of ROIs 2, 5 and 6 illustrating morphology and close proximity between presynaptic boutons (red) and postsynaptic spines (green). Intensity distributions along scan lines (dashed) plotted below. Note spatial overlap between red and green profiles as expected for apposed structures and image dimensions near the diffraction limit. Scale bars, 1 μm. (c) Representative responses from a single synapse. Presynaptic sypHTomato (top) responded to 40 stimuli and subsequent NH_4Cl challenge; postsynaptic GCaMP3 responded to the same 40 stimuli and Ca^{2+} permeabilization with ionomycin (Iono., bottom). Black traces, average responses to five trials of 40 stimuli. (d) Amplitude of peak responses of sypHTomato upon NH_4Cl challenge plotted against corresponding peak amplitudes of GCaMP3 responses in the presence of ionomycin. Data from individual pairs of neurons (7 pairs) were normalized by largest response for each pair, then pooled together.

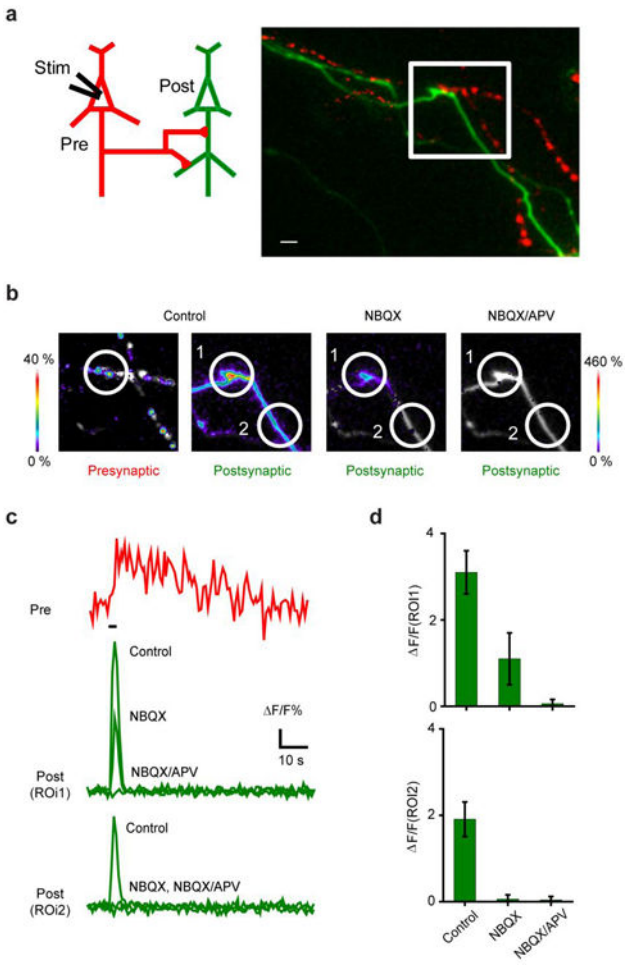

Figure 4. Dynamic imaging of synaptic transmission in suprathreshold or subthreshold condition by presynaptic sypHTomato and postsynaptic GCaMP3

(a) A cartoon diagram showing a connected pair of neurons (left). An experimental image (right) showing the spatial arrangements between presynaptic sypHTomato signal (red) and postsynaptic neuron (green) under study. Scale bar, 1 μm. (b) Pseudocolor snapshots from rectangular region in Fig (a) showing peak responses by 40 stimuli at 20 Hz from sypHTomato and GCaMP3 channel, respectively. Note the close proximity between presynaptic sypHTomato and postsynaptic GCaMP3 signal in ROI1. ROI2 shows a neighboring region of postsynaptic dendrite lacking presynaptic contact. (c) Quantification of time lapse results from Fig. (b) in control, NBQX and NBQX/APV conditions (see Methods). Scale bar, ΔF/F, 15% for sypHTomato, 60% for GCaMP3. (d) Quantification of group data from multiple pairs of connected neurons, similar to experiments shown in b and c (n =5 pairs for NBQX condition, n=11 for both control and NBQX/APV conditions). ROI 2 were typically 4 -7 μm away from ROI1.

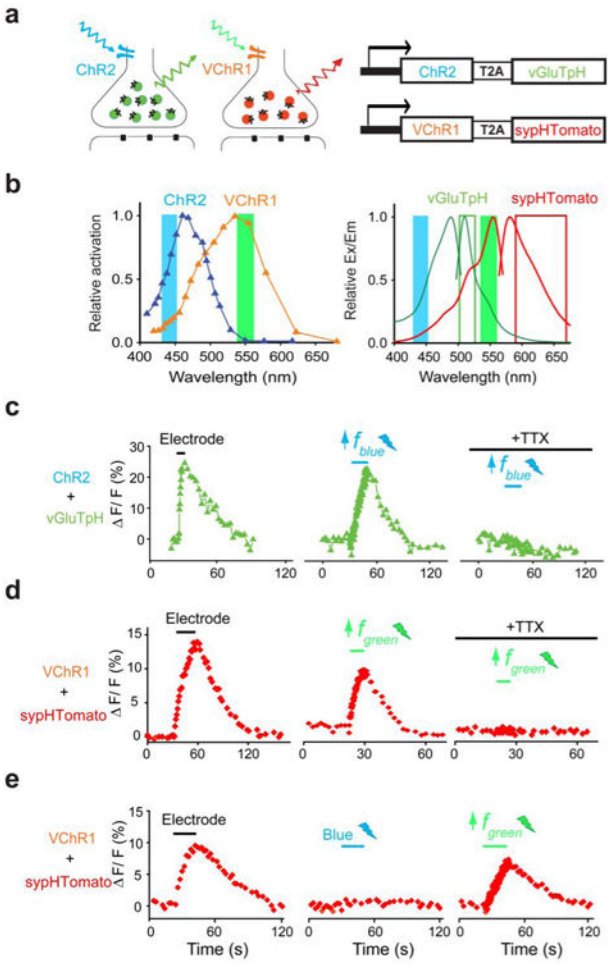

Figure 5. Proof-of-principle of an all-optical control and readout system

(a) Schematic illustrating how sypHluorin and sypHTomato can work in a multiplex way in conjunction with variants of channelrhodopsin joined in tandem by T2A linkers. (b) The activation spectra of ChR2 and VChR1 (left[10]) show extensive overlap with the excitation spectra of sypHluorin or sypHTomato (right). Filled blue and green bars show the spectra of light (426-450 nm or 546-566 nm) used to activate ChR2 and VChR1, respectively. The same light was used to excite vGluTpH and sypHTomato, respectively. Green and orange rectangles indicate the emission filter for vGlutpH and sypHTomato, respectively. (c) Expression of ChR2-T2A-vGluTpH leads to robust blue light-dependent exocytosis (center), similar to direct electrical stimulation (left). TTX abolished the light-dependent response (right), demonstrating the requirement for excitability and subsequent opening of voltage-gated calcium channels. (d) Similar and complementary experiments using VChR1-T2A-sypHTomato. (e) Blue light was unable to activate vChR1 to evoke sypHTomato responses (center) while both green light (right) and electric stimulation (left) induced robust responses. Importantly, crosstalk is not an issue for the opposite combination because green light overlaps minimally with the ChR2 activation spectrum and with pHluorin's excitation spectrum (Fig. 5b). Results shown are data from single neuron (average responses from 100 to 150 boutons). Experiments were repeated in 4-7 neurons for each condition.